Available online at www.sciencedirect.com
SCIENCE DIRECT®
Composite Structures 67 (2005) 85–97
COMPOSITE STRUCTURES
www.elsevier.com/locate/compstruct

# A combined theoretical and experimental investigation on free vibration of thin symmetrically laminated anisotropic plates

Reaz A. Chaudhuri [a,*], K. Balaraman [b], Vincent X. Kunukkasseril [b]

[a] Department of Materials Science and Engineering, University of Utah, 1222 S. Central Campus Drive, Room 304, Salt Lake City, UT 84112-0560, USA
[b] Department of Aerospace Engineering, Indian Institute of Technology, Chennai 600 036, India
Available online 26 February 2004

**Abstract**

A generalized boundary-continuous displacement based double Fourier series solution to the boundary-value problem of free vibration of thin anisotropic fiber reinforced plastic (FRP) rectangular plates is presented. The transverse vibrational characteristics of laminated anisotropic plates with arbitrary combinations of admissible boundary conditions are theoretically investigated. Numerical results presented here pertain to the natural or resonant frequencies of five-layer symmetric cross-ply plates with all edges clamped, and rotated cross-ply anisotropic plates with all edges simply supported, which are, in turn compared with the corresponding experimental results for two sets of glass fiber reinforced plastic (GFRP) thin anisotropic rectangular plates, fabricated using two different techniques. The influence of possible defects generally encountered in the fabrication process on the experimentally obtained resonant frequencies is also discussed here.


*Keywords:* FRP; GFRP; Method of fabrication; Laminated anisotropic; Cross-ply; Rotated cross-ply; Resonant frequency; Experimental method; Generalized boundary-continuous displacement based Fourier series

## 1. Introduction

Free vibration response analysis of thin anisotropic plates, fabricated with fiber reinforced composite materials such as glass/epoxy, graphite/epoxy, carbon/carbon, boron/epoxy, Kevlar-49/epoxy, etc., is of intense interest to aerospace engineers [1]. A variety of factors, such as high strength-to-weight and stiffness-to-weight ratios (resulting in fuel economy), corrosion resistance, longer fatigue life and stealth characteristics (of military aircraft, e.g., B-2 bomber, Nighthawk F117-A fighter) are responsible for increased usage of fiber reinforced composite laminates in aerospace structural applications. A more recent advancement in composites in the commercial aircraft sector, e.g., all-composite empennages on the Boeing 7J7 and McDonnell Douglas MD-91X, is to limit sonic fatigue caused by the new fuel efficient propfan or unducted fan (UDF) engines. All these advancements and design requirements place a premium on an in-depth understanding of the response characteristics of such structural components. The present study is intended to capture some of these intricacies of the dynamic response of composite structural components through analysis of a model problem—free vibration of a thin anisotropic rectangular plate. The Kirchhoff hypothesis provides a well established framework for computing through-thickness-averaged response quantities, such as deflections, stress resultants, stress couples (moment resultants), natural frequencies, buckling loads, etc., of thin plates made of composite materials.

Derivation of analytical (e.g., Fourier series) solution for the problem of an anisotropic plate is fraught with many complexities, such as those introduced by bending–twisting coupling and more important, general admissible boundary conditions, that cannot be handled by traditional analytical approaches, such as almost two centuries-old Navier's and close to a century-old Levy's. Green and Hearmon [2] introduced a boundary-continuous displacement type Fourier series method (see [3]) to solve the problem of a thin anisotropic plate subjected to simply supported boundary conditions prescribed at all four edges. The first objective of the

* Corresponding author. Tel.: +1-801-581-6282/6863; fax: +1-801-581-4816.
*E-mail address:* r.chaudhuri@m.cc.utah.edu (R.A. Chaudhuri).

0263-8223/$ - see front matter © 2004 Elsevier Ltd. All rights reserved.
doi:10.1016/j.compstruct.2004.01.001

**Nomenclature**

| | |
|---|---|
| $a$, $b$ | length and width, respectively, of a rectangular plate |
| $a_s, \ldots \bar{d}_r$ | boundary Fourier coefficients |
| $D_{ij}$ | bending and twisting rigidities |
| $f_i$ | natural or resonant frequency (Hz) |
| $h$ | total thickness of a laminated plate |
| $M_1$, $M_2$, $M_6$ | stress couples (moment resultants) |
| $m$, $n$ | number of terms in Fourier series |
| $Q_1$, $Q_2$ | shear stress resultants |
| $r$, $s$ | number of terms in Fourier series |
| $t$ | time |
| $u_3$ | transverse displacement component |
| $W_{rs}$ | plate Fourier coefficients |
| $x_1$, $x_2$, $x_3$ | Cartesian coordinate system |
| $\phi'$ | fiber orientation angle of fiber reinforced plastic anisotropic plate |
| $\rho$ | plate aspect ratio (a/b) |
| $\rho_0$ | volume density of a fiber reinforced lamina material |
| $\omega$ | natural or resonant circular frequency (rad/s) |

present investigation is to theoretically show that this method can easily be extended or generalized to solve laminated anisotropic plate boundary-value problems with other types of boundary conditions, such as all edges clamped or all edges free or some arbitrary combinations, e.g., cantilever and propped cantilever. It may be noted here that Bert and Mayberry [4], and Ashton and Waddoups [5] were the first to use approximate Raleigh–Ritz technique to solve the problem of laminated anisotropic plates. Whitney [6] presented a boundary discontinuous type double Fourier series based analytical solution for an anisotropic plate with all edges clamped using two series, and compared his results with those due to the Ritz method computed by Ashton and Waddoups [5].

A review of the literature further reveals that although a few experimental investigations and the comparisons of experimentally determined natural or resonant frequencies with their counterparts computed using approximate Raleigh–Ritz technique have been reported in the published literature, e.g., Bert and Mayberry [4], and Ashton and Waddoups [5], few authors have presented comparisons of natural frequencies computed using sophisticated analytical techniques, such as the boundary-continuous displacement type Fourier series method [2,3] with their experimental counterparts. Additionally, fabrication of model composite anisotropic plates has not been most often a part of the experimental effort. Consequently, the effect of factors influenced by the fabrication processes on the experimental results have rarely been considered. The second and more important objective of the present study is to address this important issue.

## 2. Statement of the problem

A rectangular Cartesian coordinate system ($x_1$, $x_2$ and $x_3$ axes) is considered to represent the plate geometry as shown in Fig. 1. The $x_1$–$x_2$ plane is placed at mid-depth

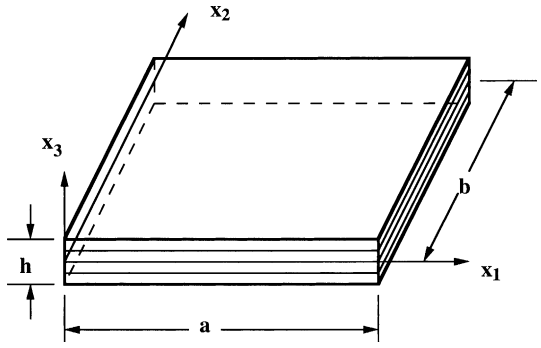


Fig. 1. A typical thin rectangular laminated plate.

(reference surface) of the plate of thickness $h$, while axis $x_3$ is normal to it. The equations of motion for a symmetrically laminated anisotropic plate can be written as follows:

$$M_{1,11} + 2M_{6,12} + M_{2,22} = \bar{\rho}\frac{\partial^2 u_3}{\partial t^2}; \tag{1}$$

where the stress couples or moment resultants, $M_1$, $M_2$ and $M_6$ are given by

$$M_1 = -(D_{11}u_{3,11} + D_{12}u_{3,22} + 2D_{16}u_{3,12}); \tag{2a}$$

$$M_2 = -(D_{12}u_{3,11} + D_{22}u_{3,22} + 2D_{26}u_{3,12}); \tag{2b}$$

$$M_6 = -(D_{16}u_{3,11} + D_{26}u_{3,22} + 2D_{66}u_{3,12}); \tag{2c}$$

and the area density of the laminated plate material is

$$\bar{\rho} = \sum_{k=1}^{N} \int_{x_3^{(i-1)}}^{x_3^{(i)}} \rho_0 \, \mathrm{d}x_3; \tag{3}$$

in which $\rho_0$ is the volume density of a fiber reinforced layer material. $u_3$ denotes transverse displacement (deflection) along $x_3$-axis, while $D_{ij}$ $(i, j = 1, 2, 6)$ are bending/twisting rigidities, respectively (see [7] for definition).

On substitution of Eq. (2) into Eq. (1), the governing partial differential equations for a symmetrically laminated anisotropic plate may be expressed in terms of the

transverse displacement component and its derivatives in the following single equation:

$$D_{11}u_{3,1111} + 4D_{16}u_{3,1112} + 2(D_{12} + 2D_{66})u_{3,1122} + 4D_{26}u_{3,1222} + D_{22}u_{3,2222} = -\bar{\rho}\frac{\partial^2 u_3}{\partial t^2}. \quad (4)$$

The following boundary conditions, prescribed at an edge $x_1 = 0$ or $a$, and their counterparts prescribed at one or both of the other two edges, form along with the governing PDE's (1)–(3) a self-adjoint differential system:

(i) Simply supported edge (SS):

$$u_3 = M_1 = 0; \quad (5a)$$

(ii) Clamped edge (CE):

$$u_3 = u_{3,1} = 0; \quad (5b)$$

(iii) Free edge (F):

$$\overline{Q}_1 = M_1 = 0; \quad (5c)$$

(iv) Roller-skate edge (RS):

$$\overline{Q}_1 = u_{3,1} = 0; \quad (5d)$$

in which the effective transverse shear stress resultant on a free edge normal to the $x_1$-axis is given by

$$\overline{Q}_1 = Q_1 + M_{6,2} = M_{1,1} + 2M_{6,2}. \quad (6)$$

## 3. Double Fourier series solution subjected to admissible and complementary boundary constraints

The assumed solution function for the problem of a finite-dimensional thin anisotropic plate, posed by the governing partial differential equation (4) and boundary conditions given by one of Eq. (5) for the edges $x_1 = 0, a$, and their counterparts prescribed at the other two edges, can be selected in the most general case as

$$u_3(x_1, x_2, t) = e^{i\omega t}W(x_1, x_2); \quad (7)$$

in which, with complementary plate boundary constraint ("ordinary" discontinuity) assigned at edges, $W(x_1, x_2)$ is expanded in the following double Fourier series:

$$W(x_1, x_2) = \sum_{r=1}^{\infty}\sum_{s=1}^{\infty} W_{rs}\sin(\alpha_r x_1)\sin(\beta_s x_2); \quad 0 < x_1 < a,\ 0 < x_2 < b; \quad (8a)$$

in which

$$\alpha_r = r\pi/a, \quad \beta_s = s\pi/b, \quad (8b)$$

and $W_{rs}$ represents $r * s$ number of plate Fourier coefficients. The following will illustrate the most general procedure of (partial) differentiation of the assumed double Fourier series, given by Eq. (8a), in the presence of "ordinary" discontinuities (resulting from the above hypothesis of complementary boundary constraint) for the general (or mixed) types of prescribed boundary conditions [8].

$$W_{,1}(x_1, x_2) = \frac{1}{2}\sum_{s=1}^{\infty} a_s\sin(\beta_s x_2) + \sum_{r=1}^{\infty}\sum_{s=1}^{\infty}(\alpha_r W_{rs} + a_s\phi_r + b_s\psi_r)\cos(\alpha_r x_1)\sin(\beta_s x_2); \quad 0 \leqslant x_1 \leqslant a,\ 0 < x_2 < b; \quad (9a)$$

$$W_{,2}(x_1, x_2) = \frac{1}{2}\sum_{r=1}^{\infty} c_r\sin(\alpha_r x_1) + \sum_{r=1}^{\infty}\sum_{s=1}^{\infty}(\beta_s W_{rs} + c_r\phi_s + d_r\psi_s)\sin(\alpha_r x_1)\cos(\beta_s x_2); \quad 0 < x_1 < a,\ 0 \leqslant x_2 \leqslant b; \quad (9b)$$

$$W_{,12}(x_1, x_2) = W_{,21}(x_1, x_2) = \frac{1}{2}\sum_{r=1}^{\infty}\alpha_r c_r\cos(\alpha_r x_1) + \frac{1}{2}\sum_{s=1}^{\infty}\beta_s a_s\cos(\beta_s x_2) + \sum_{r=1}^{\infty}\sum_{s=1}^{\infty}\{\alpha_r\beta_s W_{rs} + \beta_s(a_s\phi_r + b_s\psi_r) + \alpha_r(c_r\phi_s + d_r\psi_s)\}\cos(\alpha_r x_1)\cos(\beta_s x_2); \quad 0 \leqslant x_1 \leqslant a,\ 0 \leqslant x_2 \leqslant b; \quad (9c)$$

$$W_{,111}(x_1, x_2) = \frac{1}{2}\sum_{s=1}^{\infty}\bar{a}_s\sin(\beta_s x_2) + \sum_{r=1}^{\infty}\sum_{s=1}^{\infty}[-\alpha_r^2(\alpha_r W_{rs} + a_s\phi_r + b_s\psi_r) + \bar{a}_s\phi_r + \bar{b}_s\psi_r]\cos(\alpha_r x_1)\sin(\beta_s x_2); \quad 0 \leqslant x_1 \leqslant a,\ 0 < x_2 < b; \quad (9d)$$

$$W_{,222}(x_1, x_2) = \frac{1}{2}\sum_{r=1}^{\infty}\bar{c}_r\sin(\alpha_r x_1) + \sum_{r=1}^{\infty}\sum_{s=1}^{\infty}[-\beta_s^2(\beta_s W_{rs} + c_r\phi_s + d_r\psi_s) + \bar{c}_r\phi_s + \bar{d}_r\psi_s]\sin(\alpha_r x_1)\cos(\beta_s x_2); \quad 0 < x_1 < a,\ 0 \leqslant x_2 \leqslant b; \quad (9e)$$

$$W_{,1211}(x_1, x_2) = W_{,1112}(x_1, x_2) = W_{,1121}(x_1, x_2) = W_{,2111}(x_1, x_2) = -\frac{1}{2}\sum_{r=1}^{\infty}\alpha_r^3 c_r\cos(\alpha_r x_1) + \frac{1}{2}\sum_{s=1}^{\infty}\beta_s\bar{a}_s\cos(\beta_s x_2) + \sum_{r=1}^{\infty}\sum_{s=1}^{\infty}[-\alpha_r^2\{\alpha_r\beta_s W_{rs} + \beta_s(a_s\phi_r + b_s\psi_r) + \alpha_r(c_r\phi_s + d_r\psi_s)\} + \beta_s(\bar{a}_s\phi_r + \bar{b}_s\psi_r)]\cos(\alpha_r x_1)\cos(\beta_s x_2); \quad 0 \leqslant x_1 \leqslant a,\ 0 \leqslant x_2 \leqslant b; \quad (9f)$$

$$
\begin{aligned}
&W_{,2221}(x_1,x_2)\\
&\quad = W_{,1222}(x_1,x_2) = W_{,2122}(x_1,x_2) = W_{,2212}(x_1,x_2)\\
&\quad = -\frac{1}{2}\sum_{s=1}^{\infty}\beta_s^3 a_s\cos(\beta_s x_2) + \frac{1}{2}\sum_{r=1}^{\infty}\alpha_r\bar{c}_r\cos(\alpha_r x_1)\\
&\qquad + \sum_{r=1}^{\infty}\sum_{s=1}^{\infty}[-\beta_s^2\{\alpha_r\beta_s W_{rs} + \alpha_r(c_r\phi_s + d_r\psi_s)\\
&\qquad\quad + \beta_s(a_s\phi_r + b_s\psi_r)\}\\
&\qquad + \alpha_r(\bar{c}_r\phi_s + \bar{d}_r\psi_s)]\cos(\alpha_r x_1)\cos(\beta_s x_2);\\
&\qquad 0\leqslant x_1\leqslant a,\quad 0\leqslant x_2\leqslant b;
\end{aligned}
\tag{9g}
$$

in which the unknown boundary Fourier coefficients $a_s$, $b_s$, $c_r$, $d_r$, $\bar{a}_s$, $\bar{b}_s$, $\bar{c}_r$ and $\bar{d}_r$ are as defined in Appendix A, while $\phi_i$ and $\psi_i$ are given as follows:

$$
(\phi_i,\psi_i) = \left\{\begin{array}{ll}(0,1), & i=\text{odd}\\ (1,0), & i=\text{even}\end{array}\right\}. \tag{10}
$$

The remaining partial derivatives can be obtained by termwise differentiation.

For a fourth order PDE, given by Eq. (4) representing the equation of motion of a laminated anisotropic plate, subjected to full complementary boundary constraints assigned at both ends in each direction (e.g., the edges either free or roller-skate type), the boundary Fourier coefficients, $a_s,\ldots\bar{d}_r$, number $4(r+s)$. The non-zero boundary displacements and their partial derivatives for free or roller-skate type boundary conditions are given as follows:

$$
\{W(0,x_2); W(a,x_2)\} = \frac{a}{4}\sum_{s=1}^{\infty}(\mp a_s - b_s)\sin(\beta_s x_2); \tag{11a,b}
$$

$$
\{W(x_1,0); W(x_1,b)\} = \frac{b}{4}\sum_{r=1}^{\infty}(\mp c_r - d_r)\sin(\alpha_r x_1); \tag{11c,d}
$$

$$
\{W_{,11}(0,x_2); W_{,11}(a,x_2)\} = \frac{a}{4}\sum_{s=1}^{\infty}(\mp\bar{a}_s - \bar{b}_s)\sin(\beta_s x_2); \tag{11e,f}
$$

$$
\{W_{,22}(x_1,0); W_{,22}(x_1,b)\} = \frac{b}{4}\sum_{r=1}^{\infty}(\mp\bar{c}_r - \bar{d}_r)\sin(\alpha_r x_1). \tag{11g,h}
$$

For laminated anisotropic plates with one or more edges supported (i.e., either simply supported or clamped), the number of boundary Fourier coefficients will be correspondingly reduced. For example, for a laminated anisotropic cantilever plate with the edge $x_1 = 0$ being clamped, $W(0,x_2) = 0$, which gives $a_s = -b_s$. Similarly, for the same plate with the edge $x_1 = a$ being clamped, $W(a,x_2) = 0$, which gives $a_s = b_s$. In either case, the number of unknown boundary Fourier coefficients will be $4r + 3s$. For a laminated anisotropic propped cantilever plate with the edge $x_1 = 0$, a being clamped and simply supported, respectively, $W(0,x_2) = W(a,x_2) = 0$, which gives $a_s = b_s = 0$. In that case, the number of unknown boundary Fourier coefficients will be $4r + 2s$. For a laminated anisotropic plate with the edges either clamped or simply supported, $W(0,x_2) = W(a,x_2) = W(x_1,0) = W(x_1,b) = 0$, which will render $a_s = b_s = c_r = d_r = 0$.

The next step is to introduce the assumed solution function, given by Eqs. (7), (8a) and (8b), and its appropriately derived derivatives, such as those given by Eq. (9) above into the governing partial differential equations (4), which yields the following:

$$
\begin{aligned}
&\sum_{r=1}^{\infty}\sum_{s=1}^{\infty}[F_1(r,s)\sin(\alpha_r x_1)\sin(\beta_s x_2)\\
&\quad + F_2(r,s)\cos(\alpha_r x_1)\cos(\beta_s x_2)] + \sum_{r=1}^{\infty}F_3(r)\cos(\alpha_r x_1)\\
&\quad + \sum_{s=1}^{\infty}F_4(s)\cos(\beta_s x_2) = 0;
\end{aligned}
\tag{12}
$$

in which

$$
\begin{aligned}
F_1(r,s) = {} & D_{11}\{\alpha_r^3(\alpha_r W_{rs} + a_s\phi_r + b_s\psi_r) - \alpha_r(\bar{a}_s\phi_r\\
& + \bar{b}_s\psi_r)\} + 2(D_{12}+2D_{66})\alpha_r\beta_s\{\alpha_r\beta_s W_{rs}\\
& + \beta_s(a_s\phi_r + b_s\psi_r) + \alpha_r(c_r\phi_s + d_r\psi_s)\}\\
& + D_{22}\{\beta_s^3(\beta_s W_{rs} + c_r\phi_s + d_r\psi_s)\\
& - \beta_s(\bar{c}_r\phi_s + \bar{d}_r\psi_s)\} - \bar{\rho}\omega^2 W_{rs};
\end{aligned}
\tag{13a}
$$

$$
\begin{aligned}
F_2(r,s) = {} & 4D_{16}[-\alpha_r^2\{\alpha_r\beta_s W_{rs} + \beta_s(a_s\phi_r + b_s\psi_r)\\
& + \alpha_r(c_r\phi_s + d_r\psi_s)\} + \beta_s(\bar{a}_s\phi_r + \bar{b}_s\psi_r)]\\
& + 4D_{26}[-\beta_s^2\{\alpha_r\beta_s W_{rs} + \beta_s(a_s\phi_r + b_s\psi_r)\\
& + \alpha_r(c_r\phi_s + d_r\psi_s)\} + \alpha_r(\bar{c}_r\phi_s + \bar{d}_r\psi_s)];
\end{aligned}
\tag{13b}
$$

$$
F_3(r) = 2(-D_{16}\alpha_r^3 c_r + D_{26}\alpha_r\bar{c}_r); \tag{13c}
$$

$$
F_4(s) = 2(-D_{26}\beta_s^3 a_s + D_{16}\beta_s\bar{a}_s). \tag{13d}
$$

This step yields double Fourier sine–sine and cosine–cosine series as well as single cosine Fourier series, equating the coefficients of each of which to zero will generate $2rs + r + s$ algebraic equations against $rs$ unknowns of the assumed solution, i.e., more equations than unknowns, thus denying the existence of a Fourier series type solution. Since Eq. (12) is valid in the domain (open region) of the plate, this difficulty can be alleviated by expanding $\cos(\alpha_r x_1)\cos(\beta_s x_2)$, $\cos(\alpha_r x_1)$ and $\cos(\beta_s x_2)$ in the form of Fourier sine–sine series as suggested by Green and Hearmon [2], Chaudhuri and Kabir [3], and Kabir and Chaudhuri [9–11] as follows:

$$\cos(\alpha_r x_1)\cos(\beta_s x_2) = \sum_{m=1}^{\infty}\sum_{n=1}^{\infty} h_{rm}h_{sn}\sin(\alpha_m x_1)\sin(\beta_n x_2); \quad r \neq 0,\ s \neq 0;\ 0 < x_1 < a;\ 0 < x_2 < b; \tag{14a}$$

$$\cos(\alpha_r x_1) = \sum_{m=1}^{\infty} h_{rm}\sin(\alpha_m x_1); \quad r \neq 0; \tag{14b}$$

$$\cos(\beta_s x_2) = \sum_{m=1}^{\infty} h_{sn}\sin(\beta_n x_2); \quad s \neq 0; \tag{14c}$$

with

$$h_{rm} = \begin{cases} \frac{4m}{\pi(m^2-r^2)}, & m+r = \text{odd};\ m \neq r; \\ 0, & m+r = \text{even}; \end{cases} \tag{15a}$$

$$h_{sn} = \begin{cases} \frac{4n}{\pi(n^2-s^2)}, & n+s = \text{odd};\ n \neq s; \\ 0, & n+s = \text{even}; \end{cases} \tag{15b}$$

and

$$h_{0m} = h_{0n} = 1. \tag{15c}$$

Utilization of Eqs. (14) and (15) followed by arrangement of the resulting series as a double Fourier sine–sine series, and setting the coefficient of each term to zero, yields the following set of equations for $r, s = 1, 2, 3, \ldots$ :

$$\begin{aligned} &F(r,s)W_{rs} - 4\sum_{m=1}^{\infty}\sum_{n=1}^{\infty}\alpha_m\beta_n(\gamma\alpha_m^2 + \chi\beta_n^2)h_{rm}h_{sn}W_{mn} \\ &+ 4\gamma\sum_{m=1}^{\infty}\sum_{n=1}^{\infty}[-\alpha_m^2\{\beta_n(a_n\phi_m + b_n\psi_m) + \alpha_m(c_m\phi_n \\ &+ d_m\psi_n)\} + \beta_n(\bar{a}_n\phi_m + \bar{b}_n\psi_m)]h_{rm}h_{sn} \\ &+ 4\chi\sum_{m=1}^{\infty}\sum_{n=1}^{\infty}[-\beta_n^2\{\beta_n(a_n\phi_m + b_n\psi_m) + \alpha_m(c_m\phi_n + d_m\psi_n)\} \\ &+ \alpha_m(\bar{c}_m\phi_n + \bar{d}_m\psi_n)]h_{rm}h_{sn} \\ &+ 2\left[\sum_{m=1}^{\infty}\alpha_m(\chi\bar{c}_m - \gamma\alpha_m^2 c_m)h_{rm} + \sum_{n=1}^{\infty}\beta_n(\gamma\bar{a}_n - \chi\beta_n^2 a_n)h_{sn}\right] \\ &+ 4\gamma\sum_{n=1}^{\infty}\left\{\frac{1}{2}\beta_n\bar{a}_n h_{sn} + \sum_{m=1}^{\infty}\beta_n(\bar{a}_n\phi_m + \bar{b}_n\psi_m)h_{rm}h_{sn}\right\} \\ &+ 4\chi\sum_{m=1}^{\infty}\left\{\frac{1}{2}\alpha_m\bar{c}_m h_{rm} + \sum_{n=1}^{\infty}\alpha_m(\bar{c}_m\phi_n + \bar{d}_m\psi_n)h_{rm}h_{sn}\right\} \\ &= -\alpha_r\Big\{\alpha_r^2(a_s\phi_r + b_s\psi_r) - (\bar{a}_s\phi_r + \bar{b}_s\psi_r)\Big\} \\ &\quad - 2\xi\Big\{\beta_s(a_s\phi_{r\cdot} + b_s\psi_r) + \alpha_r(c_r\phi_s + d_r\psi_s)\Big\} \\ &\quad - \eta\beta_s\Big\{\beta_s^2(c_r\phi_s + d_r\psi_s) - (\bar{c}_r\phi_s + \bar{d}_r\psi_s)\Big\}; \end{aligned} \tag{16}$$

in which

$$F(r,s) = \alpha_r^4 + 2\xi\alpha_r^2\beta_s^2 + \eta\beta_s^4 - \lambda; \tag{17}$$

with

$$\xi = (D_{12} + 2D_{66})/D_{11}; \qquad \eta = D_{22}/D_{11}; \tag{18a,b}$$

$$\gamma = D_{16}/D_{11}; \qquad \chi = D_{26}/D_{11}; \tag{18c,d}$$

and

$$\lambda = \bar{\rho}\omega^2/(D_{11}). \tag{18e}$$

Eq. (16) can be further simplified by using the following summation results [2]:

$$\frac{1}{2n^2} + \sum_{m=2,\ldots\,\text{even}}^{\infty}\frac{1}{(n^2-m^2)} = 0, \quad n = \text{odd}; \tag{19a}$$

$$\sum_{m=1,\ldots\,\text{odd}}^{\infty}\frac{1}{(n^2-m^2)} = 0, \quad n = \text{even}. \tag{19b}$$

The remaining equations are supplied by the prescribed admissible boundary conditions at each edge.

## 4. Examples of boundary conditions

The following two sets of examples are employed to illustrate the present theoretical procedure for obtaining double Fourier series solution to the problem of free vibration of a laminated anisotropic plate subjected to an arbitrary mix of admissible boundary conditions.

### 4.1. A cantilever plate

In what follows, a cantilever anisotropic plate with the edge $x_1 = 0$ clamped is considered first. The boundary conditions are given as follows:

$$W(0,x_2) = 0; \qquad W_{,1}(0,x_2) = 0; \tag{20a,b}$$

$$W_{,11}(a,x_2) + 2\gamma W_{,12}(a,x_2) + (\xi - 2\mu)W_{,22}(a,x_2) = 0; \tag{20c}$$

$$W_{,111}(a,x_2) + 4\gamma W_{,112}(a,x_2) + (\xi + 2\mu)W_{,122}(a,x_2) + 2\chi W_{,222}(a,x_2) = 0; \tag{20d}$$

$$(\xi - 2\mu)W_{,11}(x_1,0) + 2\chi W_{,12}(x_1,0) + W_{,22}(x_1,0) = 0; \tag{20e}$$

$$2\gamma W_{,111}(x_1,0) + (\xi + 2\mu)W_{,112}(x_1,0) + 4\chi W_{,122}(x_1,0) + \eta W_{,222}(x_1,0) = 0; \tag{20f}$$

$$(\xi - 2\mu)W_{,11}(x_1,b) + 2\chi W_{,12}(x_1,b) + W_{,22}(x_1,b) = 0; \tag{20g}$$

$$2\gamma W_{,111}(x_1,b) + (\xi + 2\mu)W_{,112}(x_1,b) + 4\chi W_{,122}(x_1,b) + \eta W_{,222}(x_1,b) = 0; \tag{20h}$$

in which

$$\mu = \frac{D_{66}}{D_{11}}. \tag{21}$$

On substitution of Eqs. ((11a),(f)–(h)) into Eqs. (20a,c,e,g) and noting from Eq. (9) that

$$W_{,112}(a,x_2) = W_{,222}(a,x_2) = W_{,111}(x_1,0) = W_{,122}(x_1,0) = W_{,111}(x_1,b) = W_{,122}(x_1,b) = 0; \quad (22)$$

the required number of algebraic equations are supplied by the additional boundary conditions. The final step involves expansion of cosine term in the moment boundary conditions into a sine series of the form:

$$\cos(\beta_s x_2) = \sum_{r=1}^{\infty} h_{sr} \sin(\beta_r x_2) \quad (0 < x_2 < b); \quad (23)$$

where as before

$$h_{sr} = \begin{cases} \dfrac{4r}{\pi(r^2 - s^2)}, & r+s = \text{odd}; \ \ n \neq s; \\ 0, & r+s = \text{even}. \end{cases} \quad (24)$$

### 4.2. All edges either simply supported or clamped

The boundary conditions are given as follows:

(i) *All edges simply supported*:

$$W(0,x_2) = 0; \quad (25a)$$

$$W_{,11}(0,x_2) + 2\gamma W_{,12}(0,x_2) + (\xi - 2\mu) W_{,22}(0,x_2) = 0; \quad (25b)$$

$$W(a,x_2) = 0; \quad (25c)$$

$$W_{,11}(a,x_2) + 2\gamma W_{,12}(a,x_2) + (\xi - 2\mu) W_{,22}(a,x_2) = 0; \quad (25d)$$

$$W(x_1,0) = 0; \quad (25e)$$

$$(\xi - 2\mu) W_{,11}(x_1,0) + 2\chi W_{,12}(x_1,0) + W_{,22}(x_1,0) = 0; \quad (25f)$$

$$W(x_1,b) = 0; \quad (25g)$$

$$(\xi - 2\mu) W_{,11}(x_1,b) + 2\chi W_{,12}(x_1,b) + W_{,22}(x_1,b) = 0; \quad (25h)$$

(ii) *All edges clamped*:

$$W(0,x_2) = 0; \qquad W_{,1}(0,x_2) = 0; \quad (26a,b)$$

$$W(a,x_2) = 0; \qquad W_{,1}(a,x_2) = 0; \quad (26c,d)$$

$$W(x_1,0) = 0; \qquad W_{,1}(x_1,0) = 0; \quad (26e,f)$$

$$W(x_1,b) = 0; \qquad W_{,1}(x_1,b) = 0. \quad (26g,h)$$

In both the situations of supported edges, the assumed transverse displacement solution function is given by

$$W(x_1,x_2) = \sum_{r=1}^{\infty} \sum_{s=1}^{\infty} W_{rs} \sin(\alpha_r x_1) \sin(\beta_s x_2); \quad 0 \leqslant x_1 \leqslant a; \ \ 0 \leqslant x_2 \leqslant b; \quad (27)$$

which completely satisfies the displacement boundary conditions a priori, in a manner similar to Navier's approach, while they do not satisfy the corresponding moment or slope boundary conditions for all edges simply supported or all edges clamped, respectively. The derivatives, that cannot be obtained by termwise differentiation, are given as follows:

$$W_{,11}(x_1,x_2) = -\sum_{r=1}^{\infty} \sum_{s=1}^{\infty} \alpha_r^2 W_{rs} \sin(\alpha_r x_1) \sin(\beta_s x_2); \quad 0 < x_1 < a; \ \ 0 < x_2 < b; \quad (28a)$$

$$W_{,111}(x_1,x_2) = \frac{1}{2} \sum_{s=1}^{\infty} \bar{a}_s \sin(\beta_s x_2) + \sum_{r=1}^{\infty} \sum_{s=1}^{\infty} [-\alpha_r^3 W_{rs} + \bar{a}_s \phi_r + \bar{b}_s \psi_r] \cos(\alpha_r x_1) \sin(\beta_s x_2); \quad (28b)$$

$$W_{,22}(x_1,x_2) = -\sum_{r=1}^{\infty} \sum_{s=1}^{\infty} \beta_s^2 W_{rs} \sin(\alpha_r x_1) \sin(\beta_s x_2); \quad 0 < x_1 < a; \ \ 0 < x_2 < b; \quad (28c)$$

$$W_{,222}(x_1,x_2) = \frac{1}{2} \sum_{r=1}^{\infty} \bar{c}_r \sin(\alpha_r x_1) + \sum_{r=1}^{\infty} \sum_{s=1}^{\infty} [-\beta_s^3 W_{rs} + \bar{c}_r \phi_s + \bar{d}_r \psi_s] \times \sin(\alpha_r x_1) \cos(\beta_s x_2). \quad (28d)$$

It can be easily seen that the Eq. (28) is obtained from Eq. (9) by letting unknown boundary Fourier coefficients $a_s$, $b_s$, $c_r$ and $d_r$ vanish. The procedure described above generates $2(r+s)$ unknown boundary Fourier coefficients, resulting in a total number of $rs + 2(r+s)$ unknowns in the system, which call for as many equations in order to produce a solution to the problem under investigation. The next step is to introduce the assumed solution function, given by Eq. (27), and its appropriately derived derivatives, such as those given by Eq. (28) above into the governing partial differential equations (4). This step yields double Fourier sine–sine and cosine–cosine series as before. Utilization of Eqs. (14) and (15) followed by arrangement of the resulting series as a double Fourier sine–sine series, and setting the coefficient of each term to zero, yields the following set of equations for $r, s = 1, 2, 3, \ldots$ :

$$\begin{aligned} &F(r,s) W_{rs} - 4 \sum_{m=1}^{\infty} \sum_{n=1}^{\infty} \alpha_m \beta_n (\gamma \alpha_m^2 + \chi \beta_n^2) h_{rm} h_{sn} W_{mn} \\ &+ 4\gamma \sum_{n=1}^{\infty} \left\{ \frac{1}{2} \beta_n \bar{a}_n h_{sn} + \sum_{m=1}^{\infty} \beta_n (\bar{a}_n \phi_m + \bar{b}_n \psi_m) h_{rm} h_{sn} \right\} \\ &+ 4\chi \sum_{m=1}^{\infty} \left\{ \frac{1}{2} \alpha_m \bar{c}_m h_{rm} + \sum_{n=1}^{\infty} \alpha_m (\bar{c}_m \phi_n + \bar{d}_m \psi_n) h_{rm} h_{sn} \right\} \\ &= \alpha_r (\bar{a}_s \phi_r + \bar{b}_s \psi_r) + \eta \beta_s (\bar{c}_r \phi_s + \bar{d}_r \psi_s); \end{aligned} \quad (29)$$

which is identical to its counterpart derived by Green and Hearmon [2]. Eq. (29) can be further simplified by using the summation results given by Eq. (19). The above step generates $rs$ equations. The remaining required equations numbering $2(r+s)$ may be obtained

from satisfying either (i) Eqs. (25b,d,f,h) for the case of all edges simply supported, or (ii) Eqs. (26b,d,f,h) for the case of all edges clamped.

(i) *All edges simply supported*:

Satisfying the moment boundary conditions given by Eqs. (25b,d,f,h) and subsequent elimination of the boundary Fourier coefficients $\bar{a}_s$, $\bar{b}_s$, $\bar{c}_r$ and $\bar{d}_r$ yield the following set of equations (for each $r, s = 1, 2, \ldots$) [2]:

$$F(r,s)W_{rs} - 2\sum_{m=1}^{\infty}\sum_{n=1}^{\infty}\alpha_m\beta_n\{\gamma(\alpha_m^2+\alpha_r^2) + \chi(\beta_s^2+\beta_n^2)\}h_{rm}h_{sn}W_{mn} = 0; \tag{30}$$

which can be represented in the following compact form:

$$\sum_{m=1}^{\infty}\sum_{n=1}^{\infty}\{P_{mn}^{rs} - \lambda\delta_{mn}^{rs}\}W_{mn} = 0; \tag{31}$$

where

$$P_{mn}^{rs} = \begin{cases} Q_{mn}^{rs}h_{mn}^{rs}, & m+r = \text{odd},\ \ n+s = \text{odd}; \\ 0, & m+r = \text{even},\ \text{or}\ \ n+s = \text{even}; \end{cases} \tag{32a}$$

$$P_{mn}^{rs} = \alpha_r^4 + 2\xi\alpha_r^2\beta_s^2 + \eta\beta_s^4; \tag{32b}$$

$$Q_{mn}^{rs} = -2\alpha_m\beta_n\{\gamma(\alpha_m^2+\alpha_r^2) + \chi(\beta_s^2+\beta_n^2)\}; \tag{32c}$$

$$h_{rs}^{mn} = h_{rm}h_{sn}; \tag{32d}$$

and

$$\delta_{mn}^{rs} = \begin{cases} 1, & m = r,\ \ n = s; \\ 0, & \text{otherwise}. \end{cases} \tag{32e}$$

The set of equations given by Eq. (31) can be divided into two groups: (i) $r+s =$ odd and (ii) $r+s =$ even. For non-trivial solution, the determinant corresponding to each group must vanish.

It may be noted that for a cross-ply plate ($D_{16} = D_{26} = 0$), the solution given by Eq. (30) or Eq. (31) reduces to the corresponding Navier solution ($Q_{mn}^{rs} = 0$). Further substitution of $\xi = \eta = 1$ reduces the solution to its homogeneous isotropic counterpart.

(ii) *All edges clamped*:

Satisfying the slope boundary conditions given by Eqs. (26b,d,f,h) yields the following sets of algebraic equations:

$$\sum_{r=1,\ldots\ \text{odd}}^{\infty}\alpha_r W_{rs} = 0; \qquad \sum_{r=2,\ldots\ \text{even}}^{\infty}\alpha_r W_{rs} = 0 \quad \text{for } s = 1, 2, \ldots \tag{33a,b}$$

$$\sum_{s=1,\ldots\ \text{odd}}^{\infty}\beta_s W_{rs} = 0; \qquad \sum_{s=2,\ldots\ \text{even}}^{\infty}\beta_s W_{rs} = 0 \quad \text{for } r = 1, 2, \ldots \tag{33c,d}$$

which, in conjunction with Eq. (29) will yield the required frequency determinants following the standard procedure. It may be noted that substitution of $\gamma = \chi = 0$ ($D_{16} = D_{26} = 0$) into Eq. (29), reduces it to its counterpart for a cross-ply plate. Further substitution of $\xi = \eta = 1$ reduces the solution to its homogeneous isotropic counterpart, given by Green [12].

A computer program, based upon the pivotal condensation method, has been developed to compute eigenvalues and eigenfunctions of the arbitrarily laminated plate boundary-value problem.

## 5. Experimental determination of natural frequencies

In what follows, first a novel method for fabrication of glass fiber reinforced plastic (GFRP) laminated anisotropic plates is described followed by the actual conduct of the experiment.

(i) *Fabrication of GFRP laminated anisotropic plates*:

Rotated symmetric cross-ply GFRP plates with the fiber orientation angle, $\phi'/(\pi/2+\phi')/\phi'/(\pi/2+\phi')/\phi'$, with $\phi'$ varying from 0° to 90° at an interval of 22.5° have been fabricated. The plates have been fabricated using E-glass fibers in continuous non-woven rovings form (supplied by Hindustan Pilkington) and epoxy resin mix. The resin mix is comprised of Araldite LY 556 and Hardener HY 951, both supplied by CIBA, in the ratio of 100:10 by weight. Small amounts of solvents like acetone and methyl ethyl ketone (MEK) have also been used sometimes to facilitate resin transfer in the resin transfer method discussed below. The primary innovation in the method of fabrication pertains to using wooden rectangular frames with thin nails or pins at specified spacings depending on the fiber orientation angle, shown in Fig. 2. The spacing $d$ between two contiguous fiber rovings is decided first based upon the desired fiber volume percentage ($V_f$) of a unidirectional ply or layer. As can be seen from Fig. 2(a), spacings of nails or pins, $d_x$ and $d_y$, in the $x_1$ and $x_2$ directions, respectively, on a rectangular wooden frame for lay-up of a ply with the fiber orientation angle, $\phi'$, can easily be calculated to be dcosec($\phi'$) and dsec($\phi'$), respectively. Corresponding spacings of nails or pins, $d_x'$ and $d_y'$, in the $x_1$ and $x_2$ directions, respectively, on a rectangular wooden frame for lay-up of a ply with the fiber orientation angle, $\pi/2+\phi'$, can be seen to be dsec($\phi'$) = $d_y$ and dcosec($\phi'$) = $d_x$, respectively (Fig. 2(b)). Continuous rovings either in the dry or impregnated with the resin mix are laid on the plate surface passing or wrapping around these nails or pins. Two types of techniques—the resin flow method and resin transfer method—have been implemented here, the details of which are available in Chaudhuri and Balaraman [13] and will not be repeated here. The series of plates fabricated by the resin flow and resin transfer techniques are designated C- and D-series, respectively [13]. In this study, six five-layer plates have been fabricated using

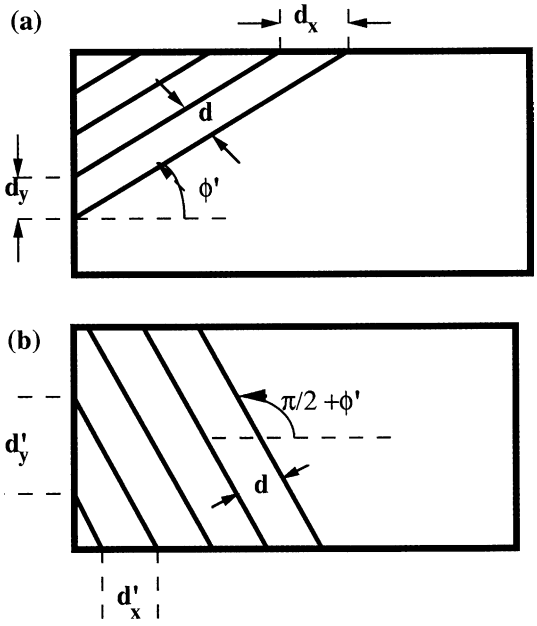


Fig. 2. Nail spacings on frames for laying up plies with fiber orientation angle (a) $\phi'$ and (b) $\pi/2+\phi'$ with respect to $x_1$-direction.

each of the techniques described above, one of which from each set has been utilized to experimentally determine the bending and twisting rigidities directly. In addition, one five-layer "defective" cross-ply [0°/90°/0°/90°/0°] D-series plate has been fabricated to experimentally assess the effect of human error, sloppiness of manufacturing, etc. on the dynamic response of the GFRP laminate.

(ii) *Experimental technique*:

The experimental set-up is shown in the accompanying photograph (Fig. 3). It involves vibrating the GFRP plate using an electrodynamic shaker or vibrator, placed underneath the plate, and connected to a variable frequency generator. The vibration output is measured using a mechanical type transducer or electrodynamic pickup, which picks up the vibration output signal, which is then amplified by an amplifier. Both the input and output signals are fed to an oscilloscope. The resonant (natural) frequency is represented by a Lissajous figure (an ellipse) on the oscilloscope screen. The mode shapes are measured by moving the transducer manually across the length and width of the plate as shown in the photograph (Fig. 3). Two types of boundary conditions have been simulated: (a) all edges simply supported and (b) all edges clamped. Fig. 3 shows a clamped plate. The simply supported boundary condition, which is usually more difficult to implement experimentally, has been simulated by creating a notch around the perimeter of the rectangular plate supported on top and bottom by knife edges (schematically shown in Fig. 4), attached to steel frames similar to its clamped edge counterpart.

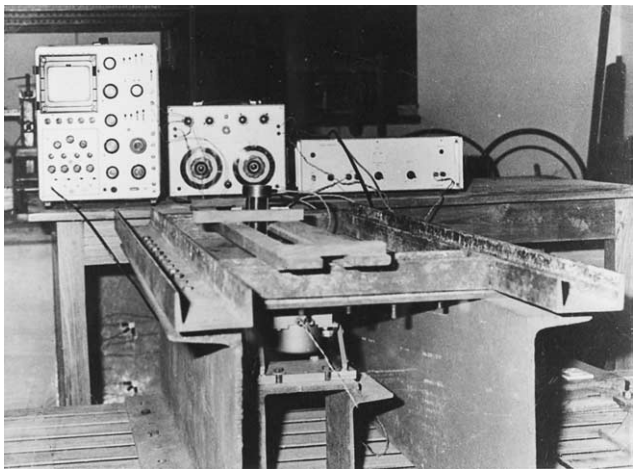

Fig. 3. Photograph of the experimental set-up for the vibration of a clamped laminate.

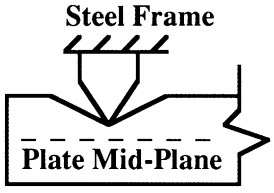


Fig. 4. Schematic diagram for a knife edge simulating a simply supported boundary condition.

## 6. Results and discussion

The length, $a$, and width, $b$, of the fiber reinforced plastic (FRP) plates tested for experimental determination of resonant frequencies are, unless otherwise stated, 820 and 420 mm, respectively. First, the bending rigidities $D_{11}$, $D_{22}$, $D_{12}$ and $D_{66}$ have directly been measured for each of the C-0° and D-0° plates by performing bending and twisting tests [14]. C-0° or D-0° is a shorthand notation for a $[\phi'/90+\phi'/\phi'/90+\phi'/\phi']$ laminate with $\phi'=0$. Also measured have been densities of each of two series of fabricated plates. These are listed in Table 1.

Tables 2 and 3 display the experimentally determined resonant frequencies and mode shapes of C-0° and D-0° symmetric cross-ply laminates with all edges clamped, and also show comparisons with their theoretical counterparts. Additionally, the lowest seven theoretical and two experimental resonant frequencies for all edges simply supported are also displayed for the purpose of comparison. As shown in Table 2, the experimentally determined fundamental frequency for a simply supported C-0° symmetric cross-ply plate is 11.75% higher than its theoretical counterpart. In contrast, the experimentally determined fundamental frequency for its clamped counterpart is within 6% of its theoretical counterpart. The agreement between experimentally and

Table 1
Properties of C- and D-series symmetric cross-ply [0/90/0/90/0] laminates

| Laminate | Thickness (mm) | Density ($10^3$ kg/m$^3$) | Volume percentage of fibers | $D_{11}$ (N m) | $D_{22}$ (N m) | $D_{12}$ (N m) | $D_{66}$ (N m) |
|---|---|---|---|---|---|---|---|
| C-0° | 8.0 | 1.274 | 11.0 | 377.69 | 200.71 | 63.37 | 61.13 |
| D-0° | 6.5 | 1.340 | 16.5 | 222.30 | 122.43 | 38.55 | 38.55 |

Table 2
Resonant frequencies and mode shape patterns of a C-series rectangular ($\rho = 1.95$) [0/90/0/90/0] symmetric cross-ply laminate

| Res. Freq. $f$ (Hz) | Mode shape ($r/s$) | Theo. (all edges SS) | Expt. (all edges SS) | Expt. (all edges C) | Theo. (all edges C) |
|---|---|---|---|---|---|
| $f_1$ | 1/1 | 50.110 | 56 | 100 | 106.335 |
| $f_2$ | 2/1 | 88.382 | 102 | 128 | 149.810 |
| $f_3$ | 3/1 | 157.247 | – | 185 | 230.878 |
| $f_4$ | 1/2 | 167.531 | – | 215 | 270.248 |
| $f_5$ | 2/2 | 200.442 | – | 240 | 306.456 |
| $f_6$ | 4/1 | 255.692 | – | 259 | 345.486 |
| $f_7$ | 3/2 | 261.614 | – | 298 | 375.046 |

Table 3
Resonant frequencies and mode shape patterns of D-series rectangular ($\rho = 1.95$) [0/90/0/90/0] symmetric cross-ply laminates

| Res. Freq. $f$ (Hz) | Mode shape ($r/s$) | Theo. (all edges SS) | Expt. (all edges SS) | Expt. (all edges C) (defective) | Expt. (all edges C) (good) | Theo. (all edges C) |
|---|---|---|---|---|---|---|
| $f_1$ | 1/1 | 42.408 | 45 | 89 | 93 | 89.513 |
| $f_2$ | 2/1 | 74.424 | 79 | 114 | 119 | 125.867 |
| $f_3$ | 3/1 | 131.687 | – | 175 | 183 | 193.532 |
| $f_4$ | 1/2 | 141.772 | – | – | 220 | 227.564 |
| $f_5$ | 2/2 | 169.633 | – | – | 252 | 258.290 |
| $f_6$ | 4/1 | 213.443 | – | – | – | 288.617 |
| $f_7$ | 3/2 | 220.998 | – | – | 300 | 315.962 |

theoretically determined resonant frequencies becomes, however, progressively worse with higher modes with the exception of the seventh mode. For example, the discrepancy for the second mode of the above simply supported C-0° symmetric cross-ply plate is 15.41%. As regards the corresponding clamped laminate, the discrepancies are 14.6%, 19.87%, 20.44%, 21.69%, 25.03% and 20.54% for the second, third, fourth, fifth, sixth and seventh mode, respectively. The reason for this discrepancy is that the interlaminar or transverse shear deformation and rotatory inertia become important even for a thin laminate like the present one as the wavelength becomes smaller with the rise of the resonant frequency.

Table 3 shows similar comparisons for a D-0° symmetric cross-ply laminate. The experimentally determined fundamental frequency for a ''good'' clamped D-0° symmetric cross-ply plate is within 4% of its theoretical counterpart. The theoretical fundamental frequency is, however, unexpectedly lower than its experimental counterpart, which is probably due to some discrepancy in manufacturing between the ''good'' D-0° laminate used for experimental determination of elastic rigidities and its counterpart for determination of natural frequencies. However, 4% difference is well within the established engineering tolerance. The experimentally determined higher resonant frequencies of the ''good'' clamped D-0° symmetric cross-ply plate are, however, lower than their theoretical counterparts, as expected. In contrast to the C-0° symmetric cross-ply laminate, the discrepancies between experimentally and theoretically determined natural frequencies, however, remain small even for higher modes. For example, the discrepancies are 5.46%, 5.44%, 3.32%, 2.44% and 5.05% for the second, third, fourth, fifth and seventh mode, respectively. The reason may be due to the fact that the D-0° symmetric cross-ply plate is thinner ($b/h = 64.62$) than the corresponding C-0° one ($b/h = 52.5$). The other reason may be attributable to the quality of fabrication of the D-0° laminate as compared to its C-0° counterpart. The resin flow method used for fabrication of C-0° plate in all likelihood left resin-rich as well as resin-starved areas, which have rendered the plate more susceptible to localized shear deformation. The ''defective'' D-0° symmetric cross-ply plate has been tested to check on this hypothesis. For example, the discrepancies between the experimentally and theoretically determined frequencies of this laminate are 9.43% and 9.58% for the second and third mode, respectively, which has partially proved the correctness of the hypothesis.

As shown in Table 3, the experimentally determined fundamental frequency and the second lowest frequency

for the simply supported "good" D-0° symmetric cross-ply laminate are 6.11% and 6.15%, respectively, higher than their theoretical counterparts. It may be remarked in this connection that the experimentally determined resonant frequencies of the simply supported cross-ply C-0° and D-0° laminates, shown in Tables 2 and 3, should have been progressively smaller than their theoretical counterparts because of the influence of the interlaminar shear deformation and rotatory inertia mentioned above. However, this decrease is more than compensated by the inability to implement ideal simply supported boundary conditions, and to prevent the occurrence of some clamping effect at the edges.

Table 4 shows comparison of the lowest two theoretical and experimental resonant frequencies for symmetric rotated cross-ply anisotropic C-series $[\phi'/90+\phi'/\phi'/90+\phi'/\phi']$ laminates, with all edges simply supported, for different angles of orientation, $\phi'$. As expected, the experimentally measured frequencies are slightly higher than their theoretically computed counterparts, because it is very difficult to simulate vanishing moment at a boundary. For example, the measured fundamental frequencies are 11.80%, 13.41%, 13.65%, 13.72% and 11.56% higher than their computed counterparts for the fiber orientation angle, $\phi' = 0°$, 22.5°, 45°, 67.5° and 90°, respectively. Likewise, the second lowest measured resonant frequencies are higher than their computed counterparts by 15.43%, 15.30%, 16.34%, 14.99% and 15.35% for the fiber orientation angle, $\phi' = 0°$, 22.5°, 45°, 67.5° and 90°, respectively. As Bert and Mayberry [4] has also noted, transverse shear flexibility, and rotatory inertia have all been neglected in the analysis, which would all tend to lower the experimental resonant frequencies of the symmetric rotated cross-ply anisotropic plates with all edges simply supported. However, as noted above, some clamping effect, which could not be eliminated in the simulation of the knife-edge (SS) boundary conditions, has contributed to higher experimental frequencies.

Fig. 5 displays comparison of theoretical and experimental (lowest two) resonant frequencies for symmetric rotated cross-ply anisotropic D-series $[\phi'/90+\phi'/\phi'/90+\phi'/\phi']$ laminates, with all edges simply supported, for different angles of orientation, $\phi'$. The agreements between the two sets of results are slightly closer for the D-series laminates than their C-series counterparts for reasons explained above. Fig. 6 exhibits the variation of the computed fundamental frequencies for symmetric rotated cross-ply anisotropic D-series $[\phi'/90+\phi'/\phi'/90+\phi'/\phi']$ laminates, with all edges simply supported, for two different aspect ratios, $\rho = a/b$, with the angle of orientation, $\phi'$. It is noteworthy from Table 4, and Fig. 5 that with aspect ratio remaining constant, the resonant frequencies corresponding to different modes vary in different fashions with respect to the angle of orientation. Also, the resonant frequency corresponding to a particular mode may vary differently with the angle of orientation for different aspect ratios.

It is further interesting to observe from Fig. 5 the occurrence of interaction modes corresponding to certain degenerate frequencies. Warburton [15] has earlier commented that such modes can occur for isotropic plates with the same boundary conditions in the $x$ and $y$ directions. Additionally, such occurrence of interaction modes for the laminates under investigation depends upon the angle of fiber orientation, $\phi'$, aspect ratio, $\rho$, and bending and twisting rigidities. Most interestingly, in such anisotropic laminates, the pair of modes, corresponding to degenerate frequencies, causing interaction modes to occur may be $r'/s' + s''/r''$ $(r', s', r'', s'' = 1, 2, 3, \ldots)$ type meaning thereby, that depending on the magnitudes of the rigidities, angle of fiber orientation and aspect ratio, any two modes can give rise to an interaction mode. This is unlike the case for an isotropic or cross-ply plate, where a typical pair is $r'/s' + s'/r'$ type.

## 7. Summary and conclusions

A generalized boundary-continuous displacement based double Fourier series solution to the boundary-value problem of free vibration of thin laminated anisotropic FRP rectangular plates is presented. The transverse vibrational characteristics of laminated anisotropic plates with arbitrary combinations of admissible boundary conditions are theoretically investigated. Numerical results presented here pertain to the natural or resonant frequencies of five-layer symmetric cross-ply plates with all edges clamped, and rotated cross-ply $[\phi'/90+\phi'/\phi'/90+\phi'/\phi']$ anisotropic plates

Table 4
Comparison of theoretical and experimental resonant frequencies for C-series rectangular ($\rho = 1.95$) symmetric rotated cross-ply anisotropic $[\phi'/90+\phi'/\phi'/90+\phi'/\phi']$ laminates for different angles of orientation, $\phi'$ (all edges simply supported)

| $f$ (Hz)\$\phi'$ | 0° | 22.5° | 45° | 67.5° | 90° |
|---|---|---|---|---|---|
| $f_1$ (Theo.) | 50.089 | 51.140 | 56.313 | 59.796 | 62.749 |
| $f_1$ (Expt.) | 56 | 58 | 64 | 68 | 70 |
| $f_2$ (Theo.) | 88.362 | 92.801 | 96.270 | 92.184 | 87.561 |
| $f_2$ (Expt.) | 102 | 107 | 112 | 106 | 101 |

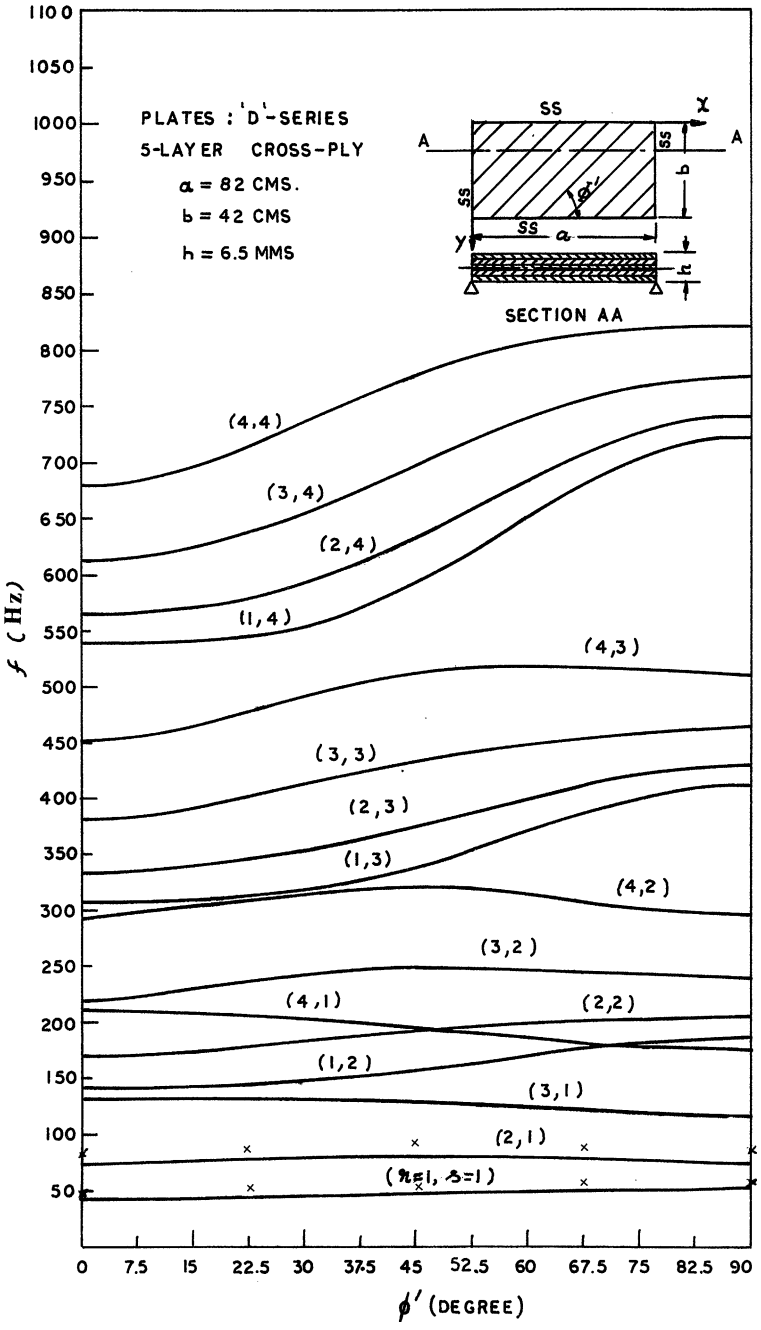


Fig. 5. Comparison of theoretical (—) and lowest two experimental (×) frequencies for symmetric rotated cross-ply anisotropic D-series rectangular ($\rho = 1.95$) $[\phi'/90 + \phi'/\phi'/90 + \phi'/\phi']$ laminates for different angles of orientation, $\phi'$ (all edges simply supported).

with all edges simply supported, which are, in turn compared with the corresponding experimental results for two sets of GFRP thin anisotropic rectangular plates, fabricated using two different techniques—(i) resin flow method and (ii) resin transfer method. The influence of possible defects generally encountered in the fabrication process on the values of the experimentally obtained natural frequencies is also discussed here. The main conclusions drawn from this study, are presented as follows:

1. Numerical results obtained for simply supported rectangular thin rotated cross-ply $[\phi'/90 + \phi'/\phi'/90 + \phi'/\phi']$ anisotropic plates show that
   (i) the occurrence of interaction modes, corresponding to certain degenerate resonant frequencies, for such plates depends upon the angle of fiber orientation, aspect ratio, and bending and twisting rigidities;
   (ii) that in such type of plates, the pair of modes causing interaction modes to occur may be

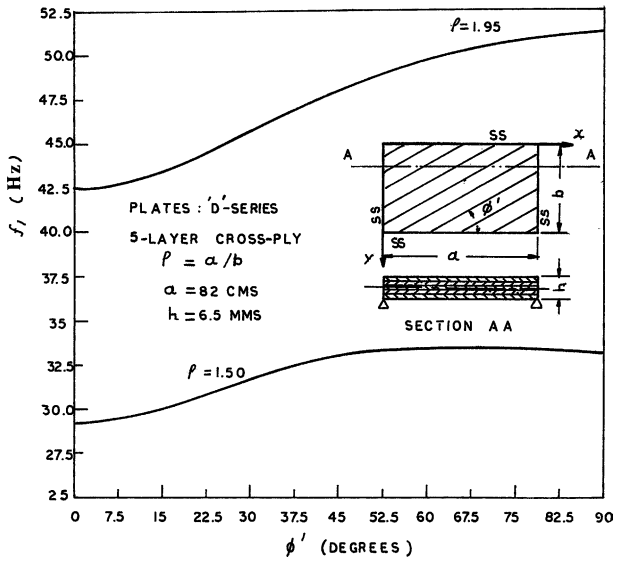


Fig. 6. Variation of the computed fundamental frequencies for symmetric rotated cross-ply anisotropic D-series $[\phi'/90+\phi'/\phi'/90+\phi'/\phi']$ laminates for two different aspect ratios with the angle of orientation, $\phi'$ (all edges simply supported).

$r'/s'+s''/r''$ $(r',s',r'',s''=1,2,3,\ldots)$ type meaning thereby, that depending on the magnitudes of the elastic rigidities, angle of fiber orientation and aspect ratio, any two modes can give rise to an interaction mode. This is unlike the case for an isotropic or cross-ply plate, where a typical pair is $r'/s'+s'/r'$ type;

(iii) that with aspect ratio remaining constant, the resonant frequencies corresponding to different modes vary in different fashions with respect to the angle of orientation. Also, the resonant frequency corresponding to a particular mode may vary differently with the angle of orientation for different aspect ratios.

2. Theoretical and experimental results for clamped rectangular thin cross-ply plates show that
   (i) the experimentally obtained resonant frequencies for all edges clamped lie, in general, between the corresponding theoretical frequencies for all edges simply supported and all edges clamped;
   (ii) the much lower percentages of error in the measured resonant frequencies of the plates made by the resin transfer method compared to those by the resin flow method can be attributed to the superiority of the former method in making a number of identical plates;
   (iii) the effect of human error and other similar factors inherent in the process of fabrication of two identical GFRP plates made by the resin transfer method do not affect their experimentally measured natural frequencies by more than 5%;
   (iv) the close agreement between theoretical and experimental resonant frequencies, for the clamped cross-ply plates made by the resin transfer method, simultaneously supports the soundness of the method of fabrication, the validity of the experimental results for the elastic rigidities and resonant frequencies as well as the theoretical results obtained by using the double Fourier series method within the framework of the classical lamination theory.
3. The experimental results for the simply supported thin rotated cross-ply $[\phi'/90+\phi'/\phi'/90+\phi'/\phi']$ anisotropic plates show that the lowest two experimentally determined resonant frequencies for different angles of fiber orientation are always, albeit slightly, higher their theoretical counterparts because of some clamping effect at the edges.

## Acknowledgements

This research was supported by an award by the Council of Scientific and Industrial Research (CSIR), Government of India, to Indian Institute of Technology, Chennai (Madras), with Professor K.A.V. Pandalai (deceased) as the Principal Investigator. The authors dedicate this paper to the loving memory of Professor Pandalai. They also gratefully acknowledge the assistance of Messrs. Anthony Joseph and Vanceslas of the workshop, Department of Aerospace Engineering in the fabrication of the FRP plates.

## Appendix A. Boundary Fourier coefficients

The boundary Fourier coefficients, arising out of ordinary discontinuities in $W(x_1,x_2)$ and its partial derivatives, are defined as follows:

$$(a_s;b_s)=\frac{4}{ab}\int_0^b[\pm W(a,x_2)-W(0,x_2)]\sin(\beta_s x_2)\,\mathrm{d}x_2; \tag{A.1a,b}$$

$$(c_r;d_r)=\frac{4}{ab}\int_0^a[\pm W(x_1,b)-W(x_1,0)]\sin(\alpha_m x_1)\,\mathrm{d}x_1; \tag{A.1c,d}$$

$$(\bar{a}_s;\bar{b}_s)=\frac{4}{ab}\int_0^b[\pm W_{,11}(a,x_2)-W_{,11}(0,x_2)]\sin(\beta_s x_2)\,\mathrm{d}x_2; \tag{A.1e,f}$$

$$(\bar{c}_r;\bar{d}_r)=\frac{4}{ab}\int_0^a[\pm W_{,22}(x_1,b)-W_{,22}(x_1,0)]\sin(\alpha_m x_1)\,\mathrm{d}x_1. \tag{A.1g,h}$$

## References

[1] Bert CW, Francis PH. Composite material mechanics: structural mechanics. AIAA J 1974;12:1173–86.

[2] Green AE, Hearmon RF. The buckling of flat rectangular plates. Philos Mag 1954;36:659–87.
[3] Chaudhuri RA, Kabir HRH. A boundary-continuous-displacement based Fourier analysis of laminated doubly-curved panels using classical shallow shell theories. Int J Eng Sci 1992;30:1647–64.
[4] Bert CW, Mayberry BL. Free vibrations of unsymmetrically laminated anisotropic plates with clamped edges. J Compos Mater 1969;3:283–92.
[5] Ashton JE, Waddoups ME. Analysis of anisotropic plates. J Compos Mater 1969;3:148–69.
[6] Whitney JM. Fourier analysis of clamped anisotropic plates. ASME J Appl Mech 1971;38:530–2.
[7] Jones RM. Mechanics of composite materials. 2nd ed. Philadelphia, PA: Taylor and Francis; 1999.
[8] Chaudhuri RA. On the roles of complementary and admissible boundary constraints in Fourier solutions to boundary-value problems of completely coupled *r*th Order P.D.E.'S. J Sound Vib 2002;251:261–313.
[9] Kabir HRH, Chaudhuri RA. Free variation of shear-flexible antisymmetric angle-ply doubly curved panels. Int J Solids Struct 1991;28:17–32.
[10] Kabir HRH, Chaudhuri RA. A generalized Navier's solution of clamped moderately thick cross-ply plates. Compos Struct 1991; 17:351–66.
[11] Kabir HRH, Chaudhuri RA. On Gibbs-phenomenon-free Fourier solution for finite shear-flexible laminated clamped curved panels. Int J Eng Sci 1994;32:501–20.
[12] Green AE. Double Fourier series and boundary value problems. Proc Cambr Philos Soc 1944;40:222–8.
[13] Chaudhuri RA, Balaraman K. A novel method for fabrication of fiber reinforced plastic laminated plates. Compos Struct (in review).
[14] Kunukkasseril VX, Chaudhuri RA, Balaraman K. A method to determine 18 rigidities of layered anisotropic plates. J Fibre Sci Tech 1975;8:303–18.
[15] Warburton GB. Discussion of: Hoffmann II, W.H. & Magness, L.S., Nodal patterns of the free flexural vibration of stiffened plates. ASME J Appl Mech 1958;25:313–4.